ture to corundum has been that a corresponding feature expected at 22 μm is not observed. However, the amplitude of the 22-μm feature is known to vary with grain shape (*37*) and is much lower in intensity than the 13-μm feature, and thus it may be too weak to resolve. Based on the structure and oblong shape of T103, crystalline corundum appears to be a likely contributor to the 13-μm feature. The assignment of the broad asymmetric feature peaking near 12 μm to amorphous Al_2O_3 is less debated, and this assignment gains further support from the amorphous nature of T96.

References and Notes

1. L. R. Nittler, *Earth Planet. Sci. Lett.* **209**, 259 (2003).
2. E. Zinner, *Annu. Rev. Earth Planet. Sci.* **26**, 147 (1998).
3. D. D. Clayton, L. R. Nittler, *Annu. Rev. Astron. Astrophys.*, **42**, 39 (2004).
4. T. J. Bernatowicz *et al.*, *Astrophys. J.* **472**, 760 (1996).
5. E. E. Salpeter, *Annu. Rev. Astron. Astrophys.* **15**, 267 (1977).
6. K. Lodders, B. Fegley, in *Astrophysical Implications of the Laboratory Study of Presolar Materials*, E. K. Zinner, Ed. (American Institute of Physics, Woodbury, NY, 1997), vol. 402, pp. 391–450.
7. A. G. G. M. Tielens, in *From Miras to Planetary Nebulae: Which Path for Stellar Evolution?*, M. O. Mennessier, A. Omont, Eds. (Editions Frontières, Gir-sur-Yvette, France, 1990), pp. 186–200.
8. H.-P. Gail, in *Astromineralogy*, T. K. Henning, Ed. (Springer-Verlag, Heidelberg, Germany, 2003), vol. 609, pp. 55–120.
9. H.-P. Gail, E. Sedlmayr, *Faraday Discussions*, **109**, 303 (1998).
10. K. S. Jeong, J. M. Winters, E. Sedlmayr, in *Asymptotic Giant Branch Stars*, A. Lebre, C. Waelkens, T. Le Bertre, Eds. (Astronomical Society of the Pacific, San Francisco, CA, 1999), pp. 233–238.
11. H. Sogawa, T. Kozasa, *Astrophys. J.* **516**, L33 (1999).
12. T. L. Daulton *et al.*, *Science* **296**, 1852 (2002).
13. T. L. Daulton, D. D. Eisenhour, T. J. Bernatowicz, R. S. Lewis, P. Buseck, *Geochim. Cosmochim. Acta* **60**, 4853 (1996).
14. T. K. Croat, T. Bernatowicz, S. Amari, S. Messenger, F. Stadermann, *Geochim. Cosmochim. Acta* **67**, 4705 (2003).
15. The term corundum refers to only rhombohedral Al_2O_3. Several forms of Al_2O_3 can be produced synthetically, but corundum is the only natural terrestrial form. All previously reported mineral classifications of presolar oxides, including corundum, spinel, and hibonite, were based on composition measurements and an assumption of the stable crystal structure. Our data demonstrate the danger of this historic assumption and argue for a return to the stricter terminology.
16. L. Nittler, C. M. O'D. Alexander, X. Gao, R. M. Walker, E. Zinner, *Astrophys. J.* **483**, 475 (1997).
17. B.-G. Choi, G. R. Huss, G. J. Wasserburg, *Science* **282**, 1282 (1998).
18. R. M. Stroud, C. M. O'D. Alexander, L. R. Nittler, *Meteoritics* **37**, A137 (2002).
19. M. R. Lee, P. A. Bland, G. Graham, *Mineral. Mag.* **67**, 581 (2003).
20. P. J. Heaney, E. P. Vicenzi, L. A. Giannuzzi, K. J. T. Livi, *Am. Mineral.* **86**, 1094 (2001).
21. Materials and methods are available as supporting material on *Science* Online.
22. L. R. Nittler, C. M. O'D. Alexander, F. Tera, *Meteor. Planet. Sci. Supp.* **36**, A149 (2001).
23. A. I. Boothroyd, I.-J. Sackmann, *Astrophys. J.* **510**, 232 (1999).
24. Subgrains in the portion of the grains destroyed by the FIB process, and thus not observed by TEM, are unlikely (*21*).
25. A. G. G. M. Tielens, C. F. McKee, C. G. Seab, D. J. Hollenbach, *Astrophys. J.* **431**, 321 (1994).
26. A. P. Jones, A. G. G. M. Tielens, D. J. Hollenbach, *Astrophys. J.* **469**, 740 (1996).
27. I. Levin, D. Brandon, *J. Am. Ceram. Soc.* **81**, 1995 (1998).
28. B. T. Draine, *Annu. Rev. Astron. Astrophys.* **41**, 241 (2003).
29. E. Dwek, S. M. Foster, O. Vancura, *Astrophys. J.* **457**, 244 (1996).
30. C. Jäger *et al.*, *Astron. Astrophys.* **401**, 57 (2003).
31. S. X. Wang, L. M. Wang, R. C. Ewing, R. H. Doremus, *J. Appl. Phys.* **81**, 587 (1997).
32. S. J. Zinkle, L. L. Snead, *Nucl. Instrum. Methods* **B116**, 92 (1996).
33. K. Lodders, B. Fegley, in *Asymptotic Giant Branch Stars*, A. Lebre, C. Waelkens, T. Le Bertre, Eds. (Astronomical Society of the Pacific, San Francisco, CA, 1999), pp. 279–289.
34. A. K. Speck, M. J. Barlow, R. J. Sylvester, A. M. Hofmeister, *Astron. Astrophys. Suppl. Ser.* **146**, 437 (2000).
35. I. R. Little-Marenin, S. D. Price, "The shapes of silicate features," *NASA Tech. Memo. 88342* (1986) pp. 137–138.
36. W. Glaccum, in *Airborne Astronomy Symposium on the Galactic Ecosystem: From Gas to Stars to Dust*, M. R. Haas, J. A. Davidson, E. F. Erickson, Eds. (Astronomical Society of the Pacific, San Francisco, CA, 1995), vol. 73, pp. 395–396.
37. G. C. Sloan, K. E. Kraemer, J. H. Goebel, S. D. Price, *Astrophys. J.* **594**, 483 (2003).
38. T. Posch *et al.*, *Astron. Astrophys.* **352**, 609 (1999).

39. This paper is dedicated to the memory of Dr. Robert M. Walker, without whom presolar oxide grains might not have been discovered. We acknowledge funding from the Office of Naval Research and NASA.

Supporting Online Material

www.sciencemag.org/cgi/content/full/305/5689/1455/DC1

Materials and Methods

References and Notes

4 June 2004; accepted 27 July 2004

Reverse Methanogenesis: Testing the Hypothesis with Environmental Genomics

Steven J. Hallam,[1] Nik Putnam,[2] Christina M. Preston,[1] John C. Detter,[2] Daniel Rokhsar,[2] Paul M. Richardson,[2] Edward F. DeLong[1]*†

Microbial methane consumption in anoxic sediments significantly impacts the global environment by reducing the flux of greenhouse gases from ocean to atmosphere. Despite its significance, the biological mechanisms controlling anaerobic methane oxidation are not well characterized. One current model suggests that relatives of methane-producing *Archaea* developed the capacity to reverse methanogenesis and thereby to consume methane to produce cellular carbon and energy. We report here a test of the "reverse-methanogenesis" hypothesis by genomic analyses of methane-oxidizing *Archaea* from deep-sea sediments. Our results show that nearly all genes typically associated with methane production are present in one specific group of archaeal methanotrophs. These genome-based observations support previous hypotheses and provide an informed foundation for metabolic modeling of anaerobic methane oxidation.

Anaerobic oxidation of methane (AOM) in marine sediments has been estimated to consume more than 70 billion kilograms of methane annually (*1*). Analyses of pore waters from methane-oxidizing sediments along continental margins have mapped extensive zones of sulfate and methane depletion, which define the geographic and geochemical boundary conditions for AOM (*2–4*). Combined geochemical and biological evidence indicate that microbial consortia, largely composed of archaea and sulfate-reducing bacteria (SRB), can couple methane oxidation to sulfate reduction (*5*, *6*). Current models suggest that methane is converted by methanotrophic archaea to carbon dioxide and reduced by-products (possibly including molecular hydrogen), which are subsequently consumed by sulfate-reducing bacteria (*6*). In anoxic deep-sea sediments, AOM catalyzes the formation of authigenic carbonates with highly depleted ^{13}C content, thereby providing an enduring geochemical signature for past and present methane oxidation (*7–9*). Microbial mediation of AOM significantly influences both local and global biological and biogeochemical processes. The process reduces methane flux to the water column, stimulates subsurface microbial metabolism, and also supports vigorous deep-sea chemolithotrophic communities that derive energy from one of its by-products, hydrogen sulfide.

Although no archaeal methanotrophs have yet been isolated in pure culture, phylogenetic, isotopic, and biochemical analyses indicate that several different methanogen-related archaeal groups are involved in AOM (*10–13*). Two groups of putative anaerobic methane-oxidizing *Archaea* (ANME-1 and

[1]Monterey Bay Aquarium Research Institute, Moss Landing, CA 95064, USA. [2]Joint Genome Institute, Walnut Creek, CA 94598, USA.

*Present address: Massachusetts Institute of Technology, Cambridge, MA 02139, USA.

†To whom correspondence should be addressed. E-mail: delong@mit.edu

ANME-2) (*10*, *11*) and several SRB groups typically occur together in methane-rich marine sediments, although environmental surveys and incubation studies have identified distinct population structures and distributions associated with specific habitats (*10*, *14*–*17*). The extent to which ANME and SRB groups cooperate in AOM is uncertain, but specific physical associations between them have been observed (*11*, *15*).

To better define the process of AOM, we used environmental genomic techniques (*18*) to analyze methane-oxidizing archaeal populations found in deep-sea methane seeps. Our samples originated from a 6- to 9-cm-deep sediment pushcore interval (PC45) obtained from the Eel River Basin off the Mendocino California coastline (*19*). Previous geochemical and chemotaxonomic analyses of the sampling site determined that ANME and SRB groups represent active and abundant members of a microbial community associated with AOM in Eel River sediments (*14*, *15*, *17*). Microbial cells, including ANME-1, ANME-2, and associated SRB, were enriched from the sediment using density centrifugation and size selection (*19*). High-molecular-weight DNA purified from this cell enrichment was used to construct several 3000– to 4000–base pair (3- to 4-kbp) insert whole-genome shotgun (WGS) libraries, and one 32- to 45-kbp insert fosmid library (*19*). A total of 111.3 million base pairs (Mbp) of DNA sequence generated from 224,736 reads (averaging 732 bp per read) was derived from the WGS libraries. Paired-end sequencing of the fosmid library generated 4.6 Mbp of DNA sequence from 7104 reads (averaging 700 bp per read). Then, 191 fosmids encompassing 7.4 Mbp of DNA were selected for subcloning and sequencing on the basis of the results of paired-end sequencing, small-subunit ribosomal RNA (SSU rRNA), and functional gene screening (*19*). Fosmid-sequencing efforts focused on archaeal clones to maximize large-insert coverage depth of ANME genomes.

The cell purification procedure used in sample preparation was intended to reduce the complexity in the original, diverse sediment-associated microbial community and to enrich for the AOM microbial consortia. Based on SSU rRNA gene representation in both the WGS and fosmid libraries, the microbial community structure was dominated by ANME-1, ANME-2, and SRB groups (Fig. 1). The dominance of ANME-1 in the purified cell population is also supported by the distribution and types of methane-oxidizing *Archaea* (MOA)–specific methyl coenzyme M reductase (MCR) subunit A (*mcrA*) genes present in the library (figs. S1 and S2) (*17*). This enrichment of ANME cells and genomic DNA facilitated detailed genomic analyses of this population subset.

ANME-1 and ANME-2 SSU rRNA and *mcrA* genes encoded on large genomic fragments formed distinct groups and subdivisions, each showing specific substitutions, transpositions, and indels. However, over the length of each fragment, gene content and operon organization were highly conserved within any given subdivision (Fig. 2 and fig. S1). In several instances, gene content was shared among fosmids from different groups containing SSU rRNA or *mcrA*, or between fosmids containing SSU rRNA and *mcrA* (Fig. 2). On average, the G+C content of ANME-1 fosmids containing SSU rRNA and *mcrA* was 45.1%, compared with 51.1% for those of ANME-2 (table S2). Subgroups of ANME-1 and ANME-2 fosmids containing SSU rRNA or *mcrA* harbored additional methanogenesis-associated genes (Figs. 2 and 3; table S2), providing linkage information used in determining the origin of related sequences in the WGS and fosmid libraries.

Surveys of the environmental libraries revealed the presence and relative abundance of many genes encoding enzymes typically associated with the methanogenic pathway (Table 1, Fig. 4, and fig. S2) (*19*–*21*). With the exception

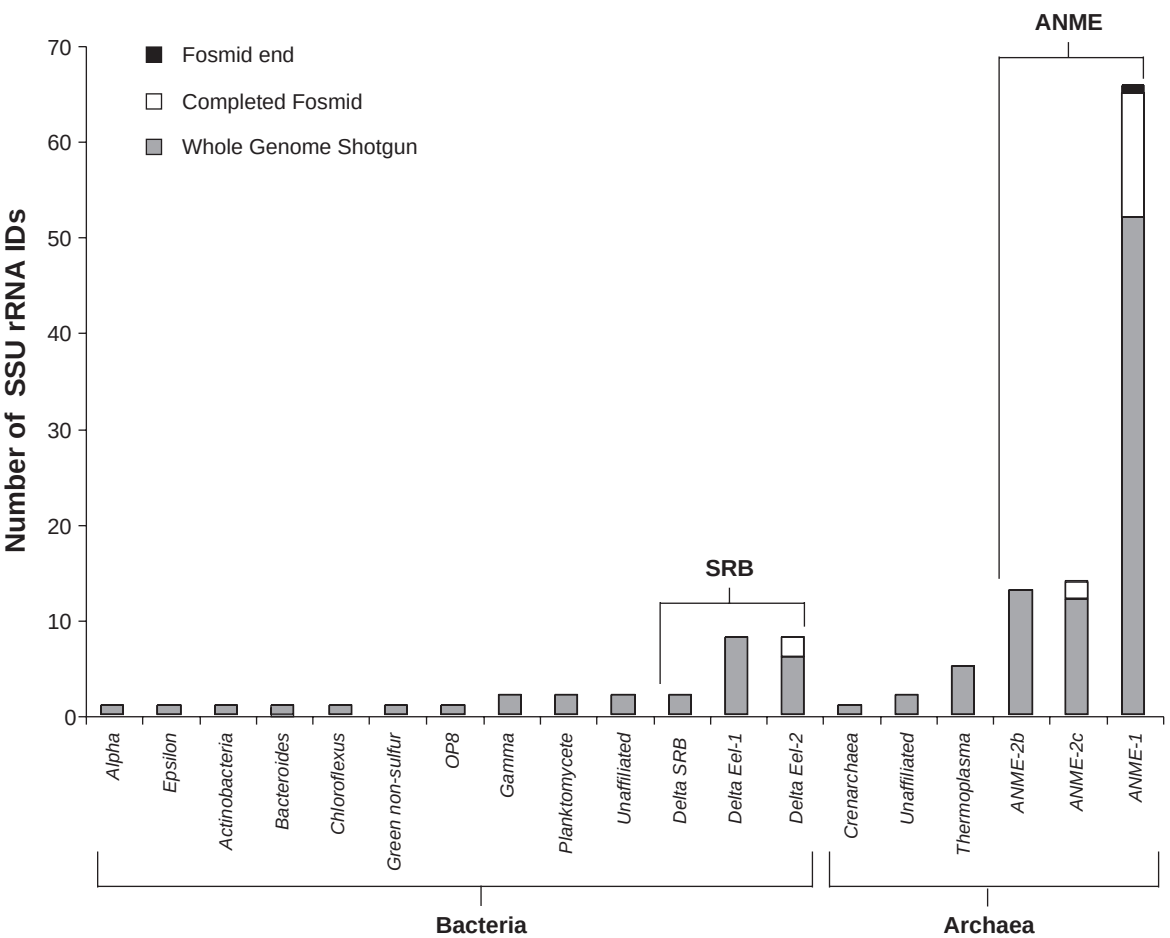

Fig. 1. Taxonomic distribution of SSU rRNA sequences identified in whole-genome shotgun sequencing (n = 114) and fosmid DNA libraries (n = 18).

of step 5, encoded by F_{420}-dependent N^5, N^{10}-methenyltetrahydromethanopterin (methylene-H4MPT) reductase (*mer*), components of all enzymatic steps (steps 1 to 4 and steps 6 to 7, Table 1) were represented in both WGS and fosmid library data sets (Table 1 and table S2). Four sequences encoding *mer* were encountered only in the WGS data set, but these probably reflect a low-level presence of bona fide methanogens in the sample. This observation is consistent with previous SSU rRNA surveys in Eel River sediments, where a few acetoclastic methanogen sequences occurred together with ANME-1 and/or ANME-2 ribotypes (*14*). Although no bona fide methanogen SSU rRNAs

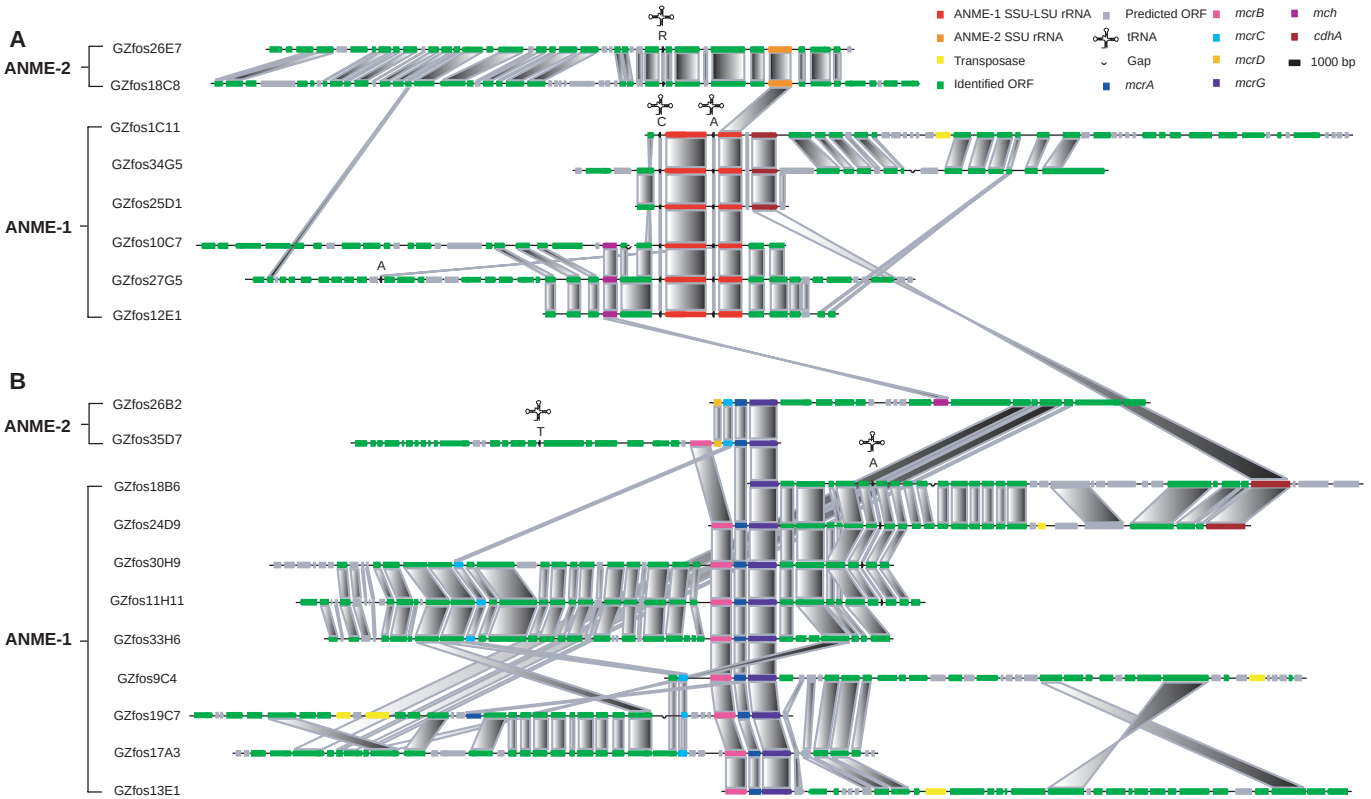

Fig. 2. Comparison of ANME-1 and ANME-2 fosmids containing SSU rRNA (**A**) or *mcrA* (**B**) based on predicted gene content and order. Genes shared in common among or between fosmids are connected by shaded boxes. ANME-1 *mcrBGA* subunits are separated from the *mcr*C component by a spacer region varying between ~1 and 14 kbp from the predicted *mcrB* start site. In every case, the *mcrC* component is linked to a tandem duplication of the *atw* locus, an adenosine 5′-triphosphate (ATP)–binding protein associated with activation of the MCR holoenzyme in vitro (*26*).

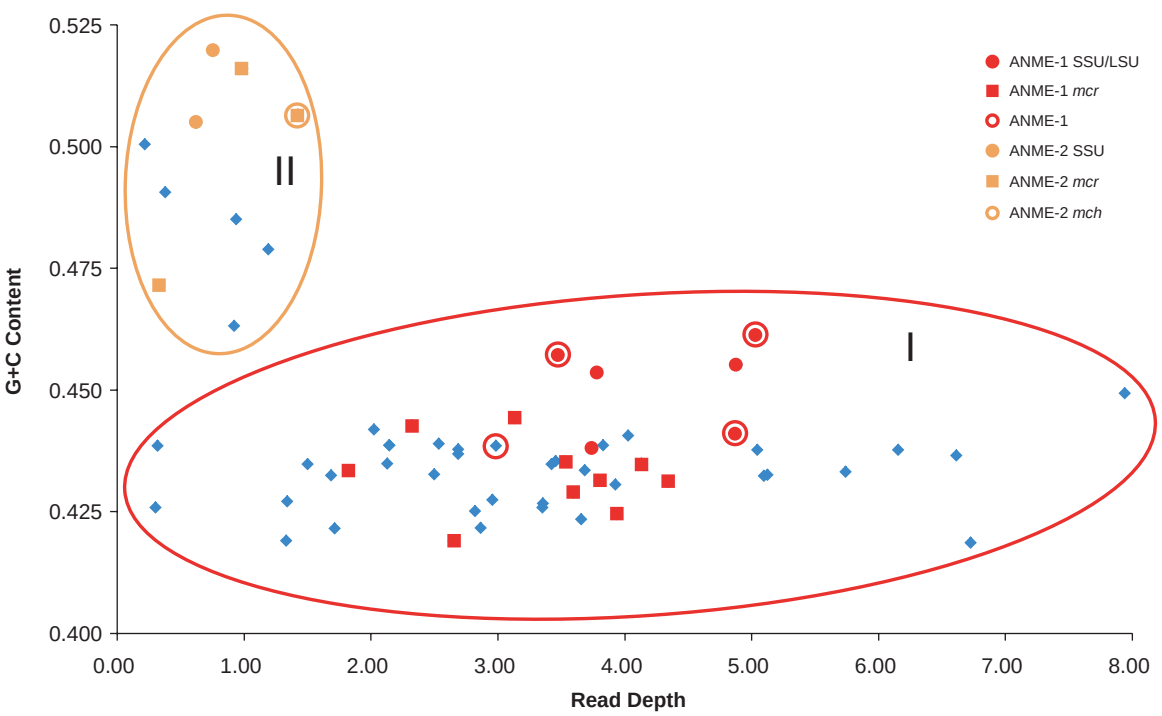

Fig. 3. Determination of ANME-1 or ANME-2 fosmid identity based on G+C content and depth of WGS coverage. Bin I bounded by red ellipse corresponds to ANME-1. Bin II bounded by orange ellipse corresponds to ANME-2. Fosmids containing SSU rRNA (filled circle), *mcr* (filled square), and *mch* (open circle) genes are highlighted in red (ANME-1) or orange (ANME-2). Read depth corresponds to the total number of WGS nucleotides aligning to a given fosmid, divided by the length (in bps) of that fosmid (*19*).

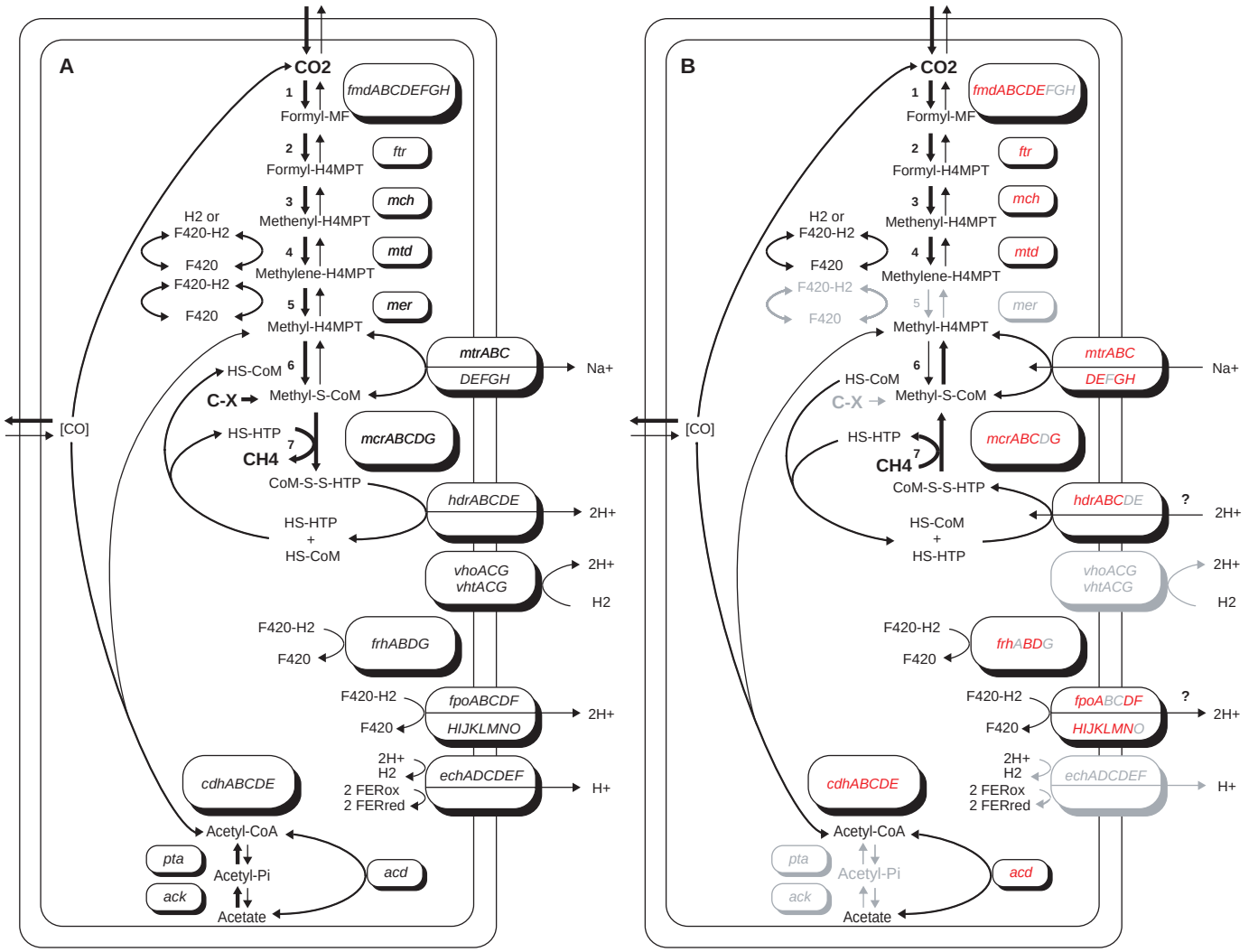

Fig. 4. Hypothetical model for reverse methanogenesis in ANME-1. (**A**) A combined pathway for methanogenesis. Gene identifications are shown in black. (**B**) A reconstructed pathway for ANME-1 based solely on predicted gene content of identified ANME-1 fosmids. Positive gene identifications are shown in red. Negative gene identifications are shown in gray.

were identified in either the WGS or fosmid library sequences, several *mcr* subunit sequences affiliated with the *Methanosarcinales* lineage were identified (fig. S2). These are readily distinguished from ANME gene fragments by both their phylogeny and WGS coverage.

Fosmid sequences were compared on the basis of their G+C content and WGS coverage (*19*). This approach was chosen on the basis of the clear G+C bias between ANME-1 and ANME-2, as well as the apparent high representation of ANME-1 genomic DNA (Fig. 1) in the WGS and fosmid libraries. Two bin distributions, I and II, were evident from using this approach (Fig. 3 and table S2). The depth of WGS coverage for bin I ranged between 0.3 and 7.9 × and between 0.4 and 1.4 × for bin II (Fig. 3). All ANME-1 fosmids containing SSU rRNA or *mcrA* mapped to bin I, and all ANME-2 fosmids containing SSU rRNA or *mcrA* mapped to bin II (Fig. 3 and table S2). Independent phylogenetic and linkage analyses clearly identified a total of 16 ANME-1 fosmids, all of which grouped in bin I (Fig. 3). Similarly, all five fosmids that could be unambiguously identified as ANME-2 grouped into bin II (Fig. 3). Assembly of binned fosmids generated 13 unique scaffolds from within bin I, and one from within bin II, with no cross-assembly between the bins (*22*). Together, these data provide strong support for the assignment of fosmids encoding methanogenesis-associated genes to ANME-1 or ANME-2 groups, according to their bin distribution. Specific identification of many ANME-1–derived genome fragments provided the framework necessary for modeling a presumptive pathway for methane consumption within this group.

The available data strongly suggest that the ANME-1 group contains all steps in the canonical seven-step methanogenic pathway with the exception of step 5, encoded by *mer* (Table 1 and Fig. 4). Although this gene is required for methanogenesis from CO_2 and one carbon (C1) compounds including methanol and methylamines, loss of *mer* activity in ANME-1 could promote AOM by increasing the activation barrier for conversion of methylene-H_4MPT to methyl-H_4MPT. Given this observation, identification of methanofuran (MF)/H_4MPT-dependent C1 transfer enzymes mediating steps 1 to 4 of methanogenesis in ANME-1 sequences is intriguing. It is possible that methylene-H_4MPT derived from reduced CO_2 becomes a substrate for assimilatory metabolism via the serine cycle (*23*). Alternatively, the C1 transfer module in ANME-1 could play a role in formaldehyde detoxification, analogous to the properties of other methylotrophic (*24*) or nonmethylotrophic bacteria (*25*).

An F_{420}-dependent quinone oxidoreductase (*fqo*) and numerous iron-sulfur cluster proteins were identified among the ANME-1

Table 1. Identification of methanogenesis-associated genes in Eel River sediment genomic DNA libraries. Step numbers indicate points in the H4MPT–dependent methanogenic pathway. Total number of gene ids among libraries: Identification based on tblastN results constrained to expectation cut-off $>E-10$. Positive identifications (ids) are indicated by numbers, and negative ids are indicated by (–) and underlined gene name and locus.

Step	Gene name	Total no. of gene ids among libraries			
		Locus	Shotgun	Fosmid ends	Completed fosmids
1	Formylmethanofuran dehydrogenase, subunit A	*fmdA*	55	12	4
	subunit B	*fmdB*	69	6	4
	subunit C	*fmdC*	50	1	4
	subunit D	*fmdD*	23	1	2
	subunit E	*fmdE*	26	2	2
	subunit F	*fmdF*	9*	2	–
	subunit G	*fmdG*	–	–	–
	subunit H	*fmdH*	–	–	–
2	Formylmethanofuran-tetrahydromethanopterin formyltransferase	*ftr*	67	7	3
3	N^5,N^{10}-methenyltetrahydromethanopterin cyclohydrolase	*mch*	29	1	5
4	F_{420}-dependent methylenetetrahydromethanopterin dehydrogenase	*mtd*	25	2	2
	H2-forming N^5,N^{10}-methylene-tetrahydromethanopterin cyclohydrolase	*hmd*	–	–	–
5	Coenzyme F_{420}-dependent N^5,N^{10}-methenyltetrahydromethanopterin reductase	*mer*‡	4	–	–
6	N^5-methyltetrahydromethanopterin-coenzyme M methyltransferase, subunit A	*mtrA*	9	–	8
	subunit B	*mtrB*	3	1	3
	subunit C	*mtrC*	10	1	3
	subunit D	*mtrD*	10	2	3
	subunit E	*mtrE*	11	–	3
	subunit F	*mtrF*	–	–	–
	subunit G	*mtrG*	7	–	4
	subunit H	*mtrH*	39	4	6
7	Methyl coenzyme M reductase, subunit α	*mcrA*	45	3	11
	subunit β	*mcrB*	28	9	11
	protein C	*mcr**C***	33	1	13
	protein D	*mcrD*	2	1	3
	subunit γ	*mcrG*	31	1	11
	Heterodisulfide reductase, subunit A	*hdrA*	319*	22	4
	subunit B	*hdrB*	80	3	8
	subunit C	*hdrC*	45	4	3
	subunit D	*hdrD*	67*	4	–
	subunit E	*hdrE*‡	7	–	–
	CO dehydrogenase/acetyl-CoA synthase, subunit α	*cdhA*	74	8	8
	subunit β	*cdhC*	52	1	3
	subunit γ	*cdhD*	38	3	1
	subunit δ	*cdhE*	56	3	4
	subunit ε	*cdhB*	16	–	4
	ADP-forming acetyl-CoA synthetase	*acd*	139†	9	4

*Includes related iron-sulfur [Fe-S] proteins. †Includes related coenzyme A-binding proteins. ‡Identified only in shotgun.

sequences (fig. S4, table S2). Moreover, electron input modules encoded by coenzyme F_{420}-reducing hydrogenase subunit B (*frhB*) were identified on 12 ANME-1 fosmids containing methanogenesis-associated genes (table S2), which suggested possible coupled expression and functioning of these enzymes, as well as the generation of a proton motive force derived from reduced F_{420} or ferredoxin. Given these observations, the "unfavorable" thermodynamics of methane activation in AOM might be overcome by metabolic coupling to the energy conservation reactions driven by the F_{420}-dependent respiratory chain. In ANME-1, *fqo* is most similar in operon structure and gene sequence to homologous genes in *Archaeoglobus fulgidus* (fig. S3), which indicates that ANME-1 contains genomic features of both sulfate-reducing and methanogenic *Archaea*.

The identification of most of the genes associated with methanogenesis in the ANME-1 group (and to a lesser extent, ANME-2) lends strong support to the reverse-methanogenesis hypothesis. The presence of genes that typify methane production in methanotrophic *Archaea* renders some of the classical molecular biomarkers of methanogenesis somewhat ambiguous. At the same time, these data provide new insight into the evolution, ecological roles, and diversity of methane-cycling *Archaea* and their unique metabolic machinery. The data also facilitate a more mechanistic biological understanding of the environmentally significant biogeochemical process of methane oxidation in anoxic marine habitats.

References and Notes

1. W. S. Reeburgh, in *Microbial Growth on C1 Compounds*, M. E. Lidstrom, F. R. Tabita, Eds. (Kluwer Academic, Dordrecht, Netherlands, 1996), pp. 334–342.
2. N. Iverson, B. B. Jorgensen, *Limnol. Oceanogr.* **30**, 944 (1985).
3. W. S. Borowski, C. K. Paull, W. Ussler III, *Mar. Geol.* **159**, 131 (1999).
4. S. D'Hondt, S. Rutherford, A. J. Spivack, *Science* **295**, 2067 (2002).
5. A. J. Zehnder, T. D. Brock, *J. Bacteriol.* **137**, 420 (1979).
6. T. M. Hoehler, M. J. Alperin, in *Microbial Growth on C1 Compounds*, M. E. Lidstrom, F. R. Tabita, Eds. (Kluwer Academic, Dordrecht, Netherlands, 1996), pp. 326–333.
7. L. D. Kulm *et al.*, *Science* **231**, 561 (1986).
8. C. K. Paull, J. P. Chanton, A. C. Neumann, J. A. Coston, C. S. Martens, *Palaios* **7** (1992).
9. G. Jiang, M. J. Kennedy, N. Christie-Blick, *Nature* **426**, 822 (2003).
10. K. U. Hinrichs, J. M. Hayes, S. P. Sylva, P. G. Brewer, E. F. DeLong, *Nature* **398**, 802 (1999).
11. A. Boetius *et al.*, *Nature* **407**, 623 (2000).
12. V. J. Orphan, C. H. House, K. U. Hinrichs, K. D. McKeegan, E. F. DeLong, *Science* **293**, 484 (2001).
13. M. Kruger *et al.*, *Nature* **426**, 878 (2003).
14. V. J. Orphan *et al.*, *Appl. Environ. Microbiol.* **67**, 1922 (2001).
15. V. J. Orphan, C. H. House, K. U. Hinrichs, K. D. McKeegan, E. F. DeLong, *Proc. Natl. Acad. Sci. U.S.A.* **99**, 7663 (2002).
16. W. Michaelis *et al.*, *Science* **297**, 1013 (2002).
17. S. J. Hallam, P. R. Girguis, C. M. Preston, P. M. Richardson, E. F. DeLong, *Appl. Environ. Microbiol.* **69**, 5483 (2003).
18. E. F. DeLong, *Curr. Opin. Microbiol.* **5**, 520 (2002).

19. Materials and methods are available as supporting material on *Science* Online.
20. J. N. Reeve, J. Nolling, R. M. Morgan, D. R. Smith, *J. Bacteriol.* **179**, 5975 (1997).
21. R. K. Thauer, *Microbiology* **144**, 2377 (1998).
22. S. J. Hallam *et al.*, data not shown.
23. S. Angelaccio *et al.*, *J. Biol. Chem.* **278**, 41789 (2003).
24. L. Chistoserdova *et al.*, *Microbiology* **146**, 233 (2000).
25. C. J. Marx, J. A. Miller, L. Chistoserdova, M. E. Lidstrom, *J. Bacteriol.* **186**, 2173 (2004).
26. C. H. Kuhner, B. D. Lindenbach, R. S. Wolfe, *J. Bacteriol.* **175**, 3195 (1993).
27. Special thanks to L. Christianson, P. Girguis, and V. Orphan at MBARI for technical assistance, and the pilots of the *ROV Tiburon* and the captain and crew of the *R/V Western Flyer*. We also thank S. Pitluck and the Joint Genome Institute staff for technical assistance, and W. Ussler and D. Graham, who provided insight and commentary. This study was supported by the David and Lucille Packard Foundation, NSF grant MCB-0236541, and the U.S. Department of Energy's Office of Science, Biological and Environmental Research Program, and the University of California, Lawrence Livermore National Laboratory, under contract W-7405-ENG-48, Lawrence Berkeley National Laboratory contract DE-AC03-765F00098, and Los Alamos National Laboratory contract W-7405-ENG-36. Sequences have been submitted to GenBank under accession numbers AY714814 to AY714873. Additional data are available at www.jgi.doe.gov/aom.

Supporting Online Material
www.science.org/cgi/content/full/305/5689/1457/DC1
Materials and Methods
Figs. S1 to S3
Tables S1 and S2
References and Notes

6 May 2004; accepted 23 July 2004

Bmp4 and Morphological Variation of Beaks in Darwin's Finches

Arhat Abzhanov,[1] Meredith Protas,[1] B. Rosemary Grant,[2] Peter R. Grant,[2] Clifford J. Tabin[1]*

Darwin's finches are a classic example of species diversification by natural selection. Their impressive variation in beak morphology is associated with the exploitation of a variety of ecological niches, but its developmental basis is unknown. We performed a comparative analysis of expression patterns of various growth factors in species comprising the genus *Geospiza*. We found that expression of *Bmp4* in the mesenchyme of the upper beaks strongly correlated with deep and broad beak morphology. When misexpressed in chicken embryos, *Bmp4* caused morphological transformations paralleling the beak morphology of the large ground finch *G. magnirostris*.

Darwin's finches are a group of 14 closely related songbird species on the Galápagos Islands and Cocos Island (*1*–*3*) collected by Charles Darwin and other members of the *Beagle* expedition in 1835 (*4*). Many biology textbooks use these birds to illustrate the history of evolutionary theory as well as adaptative radiation, natural selection, and niche partitioning (*5*–*7*). The diverse shapes and sizes of the finch beaks are believed to be maximally effective for exploiting particular types of food, including seeds, insects, and cactus flowers (*3*, *7*). The external differences in beak morphology reflect differences in their respective craniofacial skeletons (*3*, *8*). The specialized beak shapes are apparent at hatching (*3*, *8*) and thus are genetically determined.

To study the craniofacial development of Darwin's finches, we first developed a staging system by which we could compare them to each other and to the chicken, the existing avian model system (fig. S1) (*9*). We used this system to compare beak development in six species of Darwin's finches belonging to the monophyletic ground finch genus *Geospiza*. The sharp-beaked finch *G. difficilis*, with a small symmetrical beak, is the most basal species (Fig. 1A) (*10*). The other species fall into two groups: three species with broad and deep beaks used for crushing seeds (small, medium, and large ground finches—*G. fuliginosa*, *G. fortis*, and *G. magnirostris*) and cactus finches with long pointed beaks used for reaching into cactus flowers and fruits (cactus and large cactus finches—*G. scandens* and *G. conirostris*) (Fig. 1A) (*7*, *10*).

We compared beak development in embryos of all six species. Species-specific differences in the morphological shape of the beak prominence are first apparent by embryonic stage 26 (Fig. 1, B and C, and fig. S2). We therefore expected factors involved in directing the differential aspects of beak morphologies to be expressed at or before this time. We also expected such species-specific differences to reside in the mesenchyme on the basis of recent transplantation experiments between quail and duck embryos (*11*).

We analyzed expression patterns of a variety of growth factors, which are known to be expressed during avian craniofacial development (*12*–*14*), among the different *Geospiza* species, using in situ hybridizations on equivalent medial sections (as revealed by the presence of Rathke's pouch; fig. S3) of stage 26 and stage 29 embryos (Fig. 1, B and C, and fig. S4) (*15*). We looked for factors whose expression in the mesenchyme of the beak prominence correlated with the increasing depth and width of beaks seen as one compares *G. difficilis* to *G. fuliginosa*, *G. fortis*, and *G. magnirostris*. To eliminate changes in expression that were merely related to the overall size of the bird and not to changes in beak morphology, we also compared expression patterns in *G. scandens* and *G. conirostris,* which are similar in size to *G. fortis* and *G. magnirostris*, respectively, but share the more pointed beak morphology (Fig. 1A).

Most factors examined either showed no difference between Darwin's finches species (including *Shh* and *Fgf8*) (*15*) or, in the case of *Bmp2* and *Bmp7*, correlated with the size of the beak but not its shape (fig. S4). In contrast, we observed a striking correlation between beak morphology and the expression of *Bmp4* (Fig. 1, B and C). In *G. difficilis*, *Bmp4* expression is first seen at low levels in the subectodermal mesenchyme at stage 26 (Fig. 1B). Once the cartilage condensation has occurred at stage 29, *Bmp4* continues to be expressed in mesenchymal cells surrounding the most rostral part of the prenasal cartilage. When the embryos of the three ground finch species were examined, we noted a dramatic increase in the level of *Bmp4* expression in *G. magnirostris* at stage 26, whereas *Bmp4* expression in all the other species was more or less equivalent to that in *G. difficilis* (Fig. 1B). By stage 29, however, all three ground finch species displayed elevated levels of *Bmp4* expression, with *G. magnirostris* being the strongest and *G. fuliginosa* the weakest of these. *G. scandens*, a relatively pointed-beaked species of similar size to *G. fortis*, and *G. conirostris*, which is similar in size to *G. magnirostris*, did not show this increase in relative levels of *Bmp4* expression (Fig. 1C). The expression patterns of all factors were examined in three or four independent embryos for each species (except for *G. scandens*, for which two embryos were examined), and the results were consistent. Thus, the species with deeper, broader beaks relative to their length express *Bmp4* in the mesenchyme of their beak prominences at higher levels and at earlier stages (a heterochronic shift) than species with relatively narrow and shallow beak morphologies. Moreover, the differences in *Bmp4* expression are coincident with the appearance of species-

[1]Department of Genetics, Harvard Medical School, Boston, MA 02115, USA. [2]Department of Ecology and Evolutionary Biology, Princeton University, Princeton, NJ 08544, USA.

*To whom correspondence should be addressed.

Science Supporting Online Material

Reverse Methanogenesis: Testing the Hypothesis with Environmental Genomics

Steven J. Hallam, Nik Putnam, Christina M. Preston, John C. Detter, Paul M. Richardson, Daniel Rokhsar, Edward F. DeLong

doi: 10.1126/science.1100025

MATERIALS AND METHODS

Sediment sample preparation and cell enrichment

A sediment push core (PC45) was obtained from the Eel River Basin (dive T201, LAT: 40,785 LON: –124.596) at a depth of ~520 m using the remotely operated vehicle *Tiburon* (S1). Sediment samples were extruded at 3-cm intervals and frozen at –80°C until processed. Sediment from the 6- to 9-cm interval of PC45 was post-fixed in phosphate-buffered saline (PBS) and ethanol (50% 1X PBS: equal vol. ethanol) and stored at –20°C before cell enrichment and DNA extraction.

Before DNA extraction, intact cells were enriched from 40 g post-fixed sediment by Percoll gradient centrifugation and filtration. Sediment slurry (~300 μL) was added to 1.2 ml of 1X PBS, vortexed, and sonicated at 30 amps for 20 seconds on ice. Percoll density gradients were established by spinning 30 ml of 50% (vol/vol) percoll (Sigma-Aldrich) in 1X PBS solution at 17,800 rpm in an SS-34 rotor for 30 min at 4°C. Sediment slurry (3.0 ml) was loaded onto the top of each gradient. Overlain gradients were then centrifuged at 4,780 rpm in an HS-4 swinging bucket rotor for 15 min at 4°C. Following centrifugation, the entire gradient was filtered through a 3 μm polycarbonate filter (Millipore, Billerica, MA) and rinsed with 1X PBS containing 1 μM EDTA to remove excess percoll. Cells adhering to the membrane were removed in 1X PBS, pooled, pelleted in a micro-centrifuge under low gravity, and stored at –20°C before DNA extraction. Percoll-filtered samples yielded ~1.2 X 10^6 DAPI staining cells/gram starting sediment.

DNA extraction and purification

Cells (~5.1 X 10^7) were resuspended in 550 μl of Tris-EDTA pH 7.0 (TE) containing 2 mg/ml proteinase K (Fisher Scientific, Hampton, NH). SDS was added to a final concentration of 1%, and the suspension was incubated at 55°C for 20 min in a Micro 200 rotating hybridization oven (Robbins Scientific, Sunnyvale, CA). Primary incubation was followed by a second incubation at 70°C for 5 min with rotation. The crude lysate was vortexed and incubated again at 70°C for 5 min, followed by centrifugation at 10,000 rpm for 10 min to pellet cellular debris. The supernatant was removed and extracted with phenol:chloroform:IAA (25:24:1) 3 times, followed by extraction with chloroform:IAA (24:1) once to remove residual phenol. Supernatants were concentrated and washed with TE buffer (pH 7.5) in a Centricon 100 (Millipore) according to the manufacture's

instructions. Before cloning, DNA was further purified on a CsCl density gradient. Concentrated DNA was diluted to 178 μl with dH_2O and mixed with 160 mg CsCl. 10 μl of ethidium bromide (10 μg/ml) was added to the solution before centrifugation. The sample was loaded into a 7 X 20 mm polycarbonate ultracentrifuge tube (Beckman Coulter, Fullerton, CA) and centrifuged in an Optima TL Benchtop Ultracentrifuge (Beckman Coulter) at 100,000 rpm in an TLA-100 rotor for 24 hours at 20°C. Following centrifugation, the sample was visualized under UV light and resulting high-molecular-weight DNA (hmw DNA) band removed using a sterile 1-cc syringe. hwmDNA was washed 3 times with water saturated butanol to remove ethidium bromide, diluted in ~2 ml TE and concentrated in a Centricon 100 (Millipore). Approximately 3 μg hmwDNA was purified in this way.

Fosmid and shotgun library construction

Fosmids were prepared using an EpiCentre Epifos fosmid library production kit (Epicentre, Madison, WI), modifying protocols to work with reduced quantities of genomic DNA. Briefly, 600 ng (~10 g sediment equivalent) hmwDNA was end-repaired and separated on 0.5% agarose in 1X TAE o/n at 30 volts. 40-50 kbp fragment pools were gel purified and cloned into the vector pEpiFOS (Epicentre). Ligated DNA was packaged using the Epicentre MaxPlax lambda packaging extract and used to transfect *E. coli* DH10B cells. Transfected cells were selected on LB agar containing 15 μg/ml chloramphenicol. (LB_{cm15}) Resulting clones were picked into 96-well microtiter dishes containing LB_{cm15} with 7% glycerol and stored at –80 °C.

Three-kbp DNA shearing and plasmid subcloning

Approximately 1.5 μg of isolated hmwDNA or 3-5 μg of selected fosmid DNA (30 g sediment equivalent) was randomly sheared to 3- to 4-kbp fragments (25 cycles at speed code 12) in a 100 μl volume using a HydroShear™ (GeneMachines, San Carlos, CA). The sheared DNA was immediately blunt end-repaired at room temperature for 40 min using 6 U of T4 DNA Polymerase (Roche, Mountain View, CA), 30 U of DNA Polymerase I Klenow Fragment (NEB, Beverly, MA), 10 μl of 10 mM dNTP mix (Amersham Biosciences, Piscataway, NJ), and 13 μl of 10X Klenow Buffer in a 130 μl total volume. After incubation the reaction was heat inactivated for 15 min at 70°C, cooled to 4°C for 10 min and then frozen at –20 °C for storage. The end-repaired DNA was run on a 1% TAE agarose gel for ~ 30-40 min at 120 volts. Using ethidium bromide stain and UV illumination, 3- to 4-kbp fragments were extracted from the agarose gel and purified using QIAquick™ Gel Extraction Kit (QIAGEN, Valencia, CA). Approximately 200-400 ng of purified fragment was blunt-end ligated for 40 min into the Sma I site of 100 ng of pUC18 cloning vector (Roche) using the Fast-Link™ DNA Ligation Kit (Epicentre). Following standard protocols, 1 μl of ligation product was electroporated into DH10B Electromax™ cells (Invitrogen, Carlsbad, CA) using the GENE PULSER® II electroporator (Bio-Rad, Hercules, CA). Transformed cells were transferred into 1000 μl of SOC and incubated at 37 °C in a rotating wheel for 1 hour. Cells (usually 20-50 μl) were spread on 22 x 22 cm LB agar plates containing 100 μg/mL of ampicillin, 120 μg/mL of IPTG, and 50 μg/mL of X-Gal. Colonies were grown for 16 hours at 37°C. Individual white recombinant colonies were selected and picked into 384-well microtiter plates containing LB/glycerol (7.5%) media containing 50 μg/mL of ampicillin using the

Q-Bot™ multitasking robot (Genetix, Dorset, U.K.). To test the quality of the library (XYG), 24 colonies were directly PCR amplified with pUC m13 -28 and -40 primers using standard protocols. Libraries are considered to pass PCR QC if they have > 90% 3-kbp inserts (For more information go to http://www.jgi.doe.gov/).

Plasmid amplification

2 μl aliquots of saturated *E. coli* cultures (DH10B) containing pUC 18 vector with random 3- to 4-kbp DNA inserts grown in LB/glycerol (7.5%) media containing 50 μg/mL of ampicillin were added to 8 μl of a 10 mM Tris-HCl pH 8.2 + 0.1 mM EDTA denaturation buffer. The mixtures were heat lysed at 95°C for 5 min then placed at 4°C for 5 min. To these denatured products 10 μl of an RCA reaction mixture (TempliPhi™ DNA Sequencing Template Amplification Kit, Amersham Biosciences) were added. The amplification reactions were carried out at 30°C for 12-18 hours. The amplified products were heat inactivated at 65°C for 10 min then placed at 4°C until used as template for sequencing.

Sequencing and assembly

Aliquots of the 20 μl amplified plasmid RCA products were sequenced with standard M13 –28 or –40 primers. The reactions contained 1 μl RCA product, 4 pmol primer, 5 μl dH_2O, and 4 μl DYEnamic™ ET terminator sequencing kit (Amersham Biosciences). Cycle sequencing conditions were 30 rounds of 95°C-25 sec, 50°C-10 sec, 60°C-2 min, hold at 4°C. The reactions were then purified by a magnetic bead protocol (see research protocols, www.jgi.doe.gov) and run on a MegaBACE 4000 (Amersham Biosciences). Alternatively, 1 μl of the RCA product was sequenced with 2 pmol of standard M13 –28 or –40 primers, 1 μl 5X buffer, 0.8 μl H_2O, and 1 μl BigDye sequencing kit (Applied Biosystems, Foster City, CA) at 1 min denaturation and 25 cycles of 95°C-30 sec, 50°C-20 sec, 60°C-4 min, and finally hold at 4°C. The reactions were then purified by a magnetic bead protocol (see research protocols, http://www.jgi.doe.gov/) and run on an ABI PRISM 3730 (Applied Biosystems) capillary DNA sequencer.

Data analysis

Assembled shotgun reads, fosmid-ends and assembled fosmid sequences were annotated using the FGENESB pipeline for automatic annotation of bacterial genomes from Softberry (http://www.softberry.com/berry.phtml) using the following parameters and cut-offs: ORF size = 100 aa, Expectation = 1×10^{-10}. Predicted ORFs were queried against COG and GenBank non-redundant (NR) databases. To identify SSU and LSU rRNA genes, individual shotgun reads, shotgun contigs, fosmid-ends and assembled fosmid sequences were queried against NR using blastn with expectation cut-offs of 1×10^{-10}. tRNAs were identified using tRNAscan-SE 1.21 (*S2*) set to archaeal and bacterial tRNA covariance models. Automated FGENESB annotation of fosmids containing SSU rRNA or the methanogenesis-associated gene was manually refined using the genome annotation and visualization tool ARTEMIS (*S3*). Identification of methanogenesis-associated genes was based on the results of FGENESB annotation of shotgun and fosmid library sequences and tblastn queries (Table 1 and Tables S2 and S3).

Depth analysis of whole-genome shotgun (WGS) and completed fosmid clones was based on the following considerations. Given that the expected number of reads in the

WGS dataset belonging to any component genome of the environmental DNA sample mixture is proportional to both its copy number and the length of each copy, the density (or equivalently the depth of coverage) of WGS reads sampled from a given genome should provide a measure of a genome's abundance in the source material. Because MOA groups have different abundances in the source material, individual fosmid clones should be classifiable on the basis of the depth of representation of its sequence in the WGS reads. Therefore, the density of read sampling of each fosmid clone was estimated on the basis of alignment to the WGS read set. The shotgun dataset was reduced to 133,713 non-redundant reads containing at least 100 bp of high quality trimmed sequence. Vector sequence was removed from the reads using cross_match version 0.960731 (*S4*) and each read was trimmed to the longest interval over which the average phred quality score over a sliding window of 11 bp is at least 15. All reads that could be aligned over 90% of their length with a minimum percent identity threshold (*p*) of 93% were counted. The density of WGS coverage of a fosmid clone is the number of full-length WGS read hits divided by the length of the fosmid sequence. Alignments were computed using MegaBLAST version 2.2.5 (*S5*). The high degree of sequence diversity observed among and between MOA groups made the absolute values of the densities obtained sensitive to the choice of the threshold *p*. Additionally, variation among related genomic loci increased the degree of uncertainty in density estimates. Density values observed for group I, for example, had a mean and standard deviation of 5 ± 2, where we would expect perfect discrimination of alignments to yield a statistically-limited uncertainty of only 0.4, or 8%. Despite this variation, existence and composition of the two bins shown in Figure 2 was robust to the choice of the threshold p. In several instances, contigs from incomplete, but ordered and oriented fosmids were included in the depth analysis (Table S2).

Phylogenetic analysis

Phylogenetic analyses of fosmid derived SSU rRNA and *mcrA* genes were preformed on sequences from known MOA groups as well as representatives from the primary lines of descent within methanogenic lineages. SSU rRNA and *mcrA* gene sequences were identified via homology searches of the WGS and fosmid libraries (see above) and PCR-based screening (*S6*). SSU rRNA sequence data were compiled with ARB software (www.arb-home.de) and aligned with sequences from GenBank using the FastAligner program. Aligned sequences were visually inspected for conservation of secondary structure features and manually edited when necessary. SSU rRNA trees were based on comparison of 644 nucleotides. *mcrA* trees were based on comparison of 368 amino acids. Phylogenetic trees for both SSU rRNA and *mcrA* genes were generated using distance and parsimony methods implemented in PAUP* version 4.0b10 (*S7*). SSU rRNA sequence distances were estimated using the Kimura two-parameter model. Bootstrapping for distance and parsimony was accomplished with 1,000 replicates per tree using heuristic search methods.

References and Notes

S1. V. J. Orphan, C. H. House, K. U. Hinrichs, K. D. McKeegan, E. F. DeLong, *Proc. Natl. Acad. Sci. U.S.A.* **99**, 7663 (2002).
S2. http://www.genetics.wustl.edu/eddy/tRNAscan-SE

S3. K. Rutherford et al., Bioinformatics 16, 944-945 (2000).
S4. Green P., unpublished software
S5. Z. Zhang, S. Schwartz, L. Wagner, W. Miller, J Comput Biol 7, 203-14 (2000).
S6. S. J. Hallam, P. R. Girguis, C. M. Preston, P. M. Richardson, E. F. DeLong, Appl Environ Microbiol 69, 5483-91 (2003).
S7. D. L. Swafford. (Sinauer Associates, Sunderland, Massachusetts, 2000).

SUPPORTING FIGURES & LEGENDS

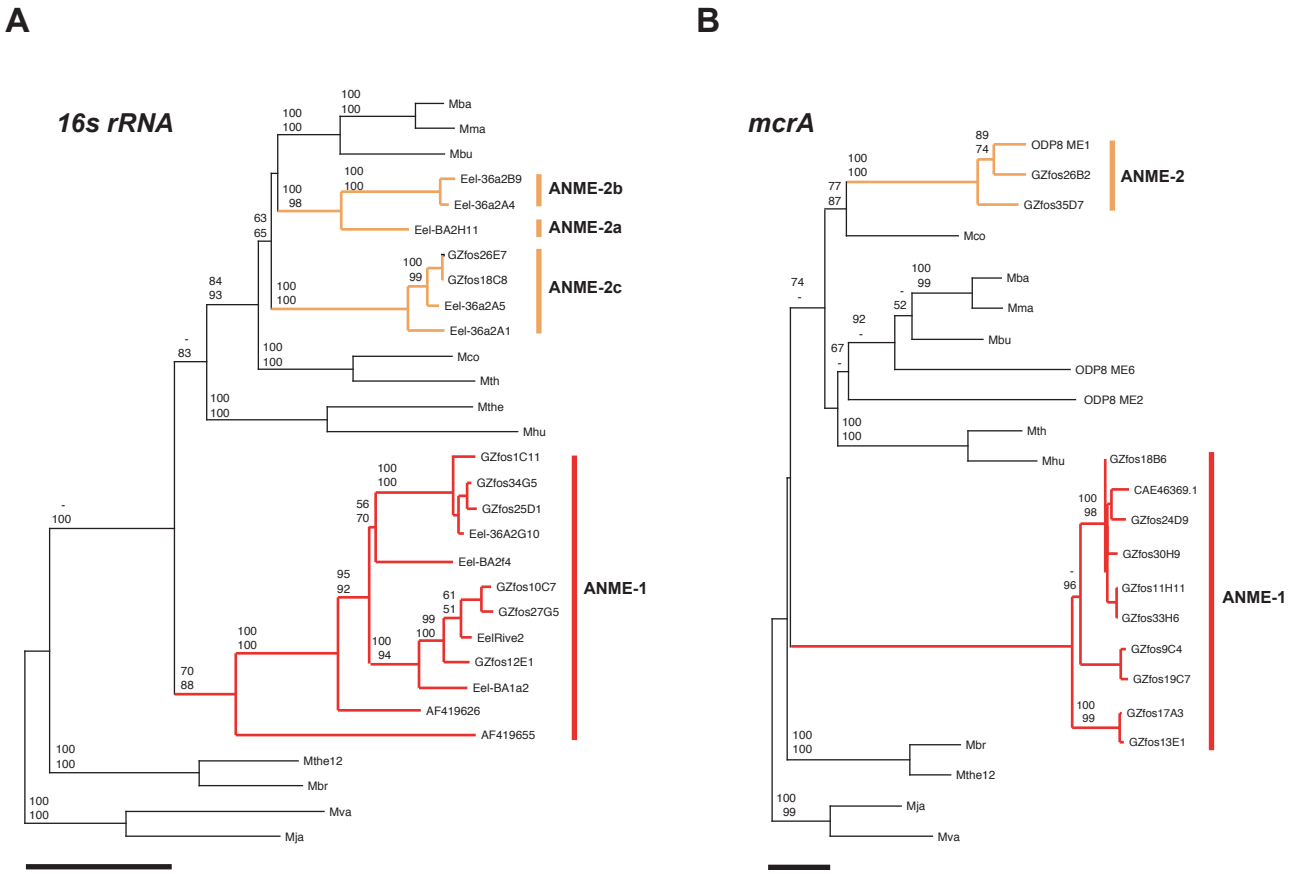

Fig. S1 Phylogentic relationship of ANME-1 and ANME-2 SSU rRNA and mcrA genes. (A) Comparison of methane-utilizing archaeal SSU rRNA sequences recovered from environmental fosmid libraries and major methanogenic lineages. (B) Comparison of methane-utilizing archaeal mcrA sequences recovered from environmental fosmid libraries and major methanogenic lineages. (A-B) Methanosarcinales: Methanococcoides burtonii (Mbu), Methanosarcina mazei (Mma), Methanosarcina barkeri (Mba), Methanosaeta concillii (Mco), Methanomicrobiales: Methanoculleus thermophilicus (Mth), Methanospirillium hungatei (Mhu). Methanobacteriales: Methanobacterium bryanti (Mbr), Methanothermobacter thermautotrophicus (Mthe12). Methanococcales: Methanocaldococcus jannaschii (Mja), Methanococcus vannielii (Mva) (see Table S1 for accession numbers). Bootstrap values are based on 1,000 replicates (neighbor joining on top and parsimony on bottom) and shown only when support is greater than 50%. Red highlights ANME-1 group sequences. Orange highlights ANME-2c group members. Scale bars represents 50 changes.

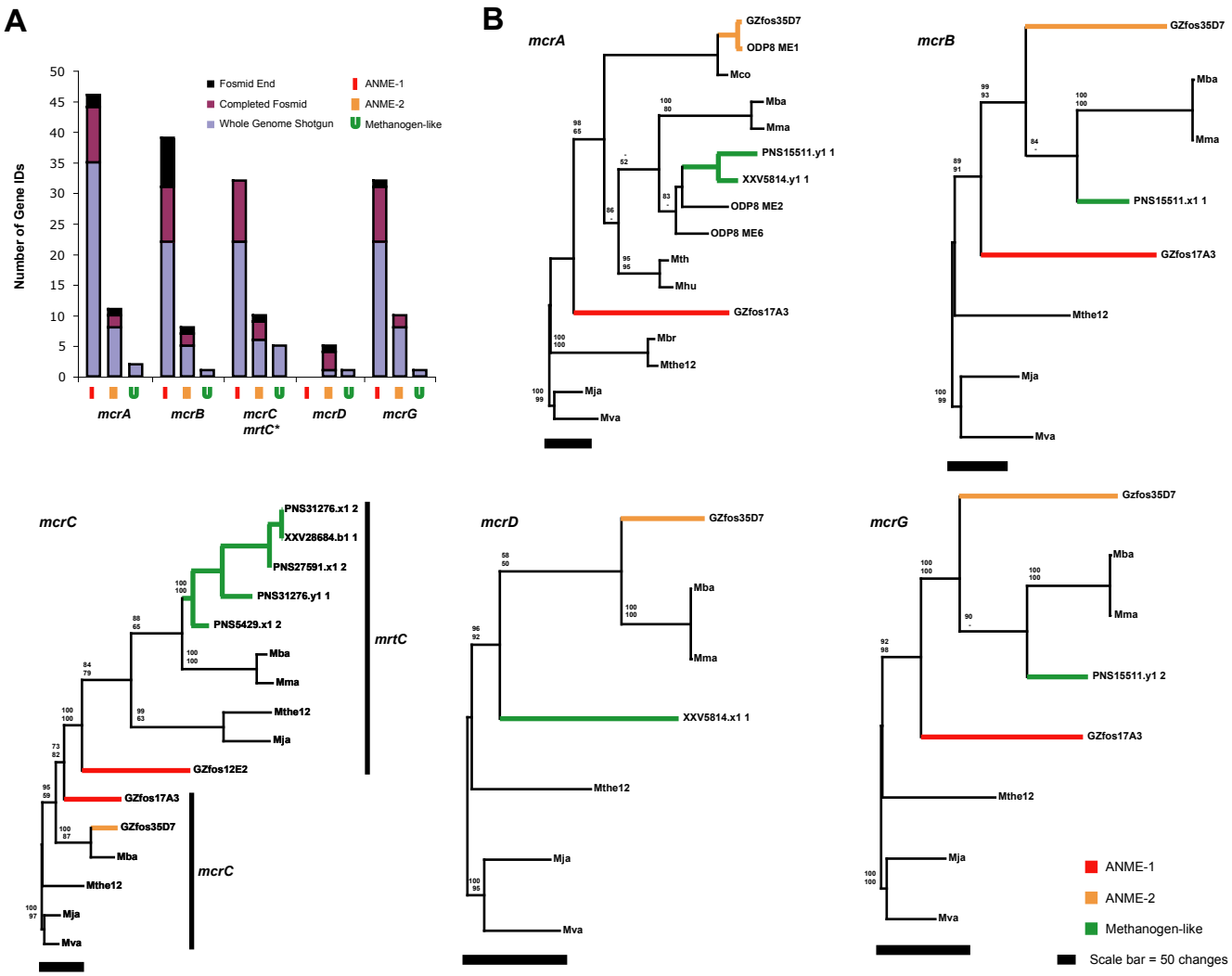

Fig. S2 Identification of methanogen-like mcr subunits in the whole genome shotgun sequences (WGS) (A) Total number of individual mcr subunit identifications and corresponding bin distributions in WGS, completed fosmid and fosmid end sequences. Methyl coenzyme M reductase protein C (mcrC) paralog mrtC included in total mcrC count. (B) Phylogenetic placement of mcr subunits grouping outside of ANME-1 and ANME-2 bins. Only one representative fosmid sequence for each ANME-1 or ANME-2 mcr subunit is included for comparison. Bootstrap values are based on 1,000 replicates (neighbor joining on top and parsimony on bottom) and shown only when support is greater than 50%. Red highlights ANME-1 group sequences. Orange highlights ANME-2c group members. Green highlights methanogen-like sequences. Scale bar represents 50 changes.

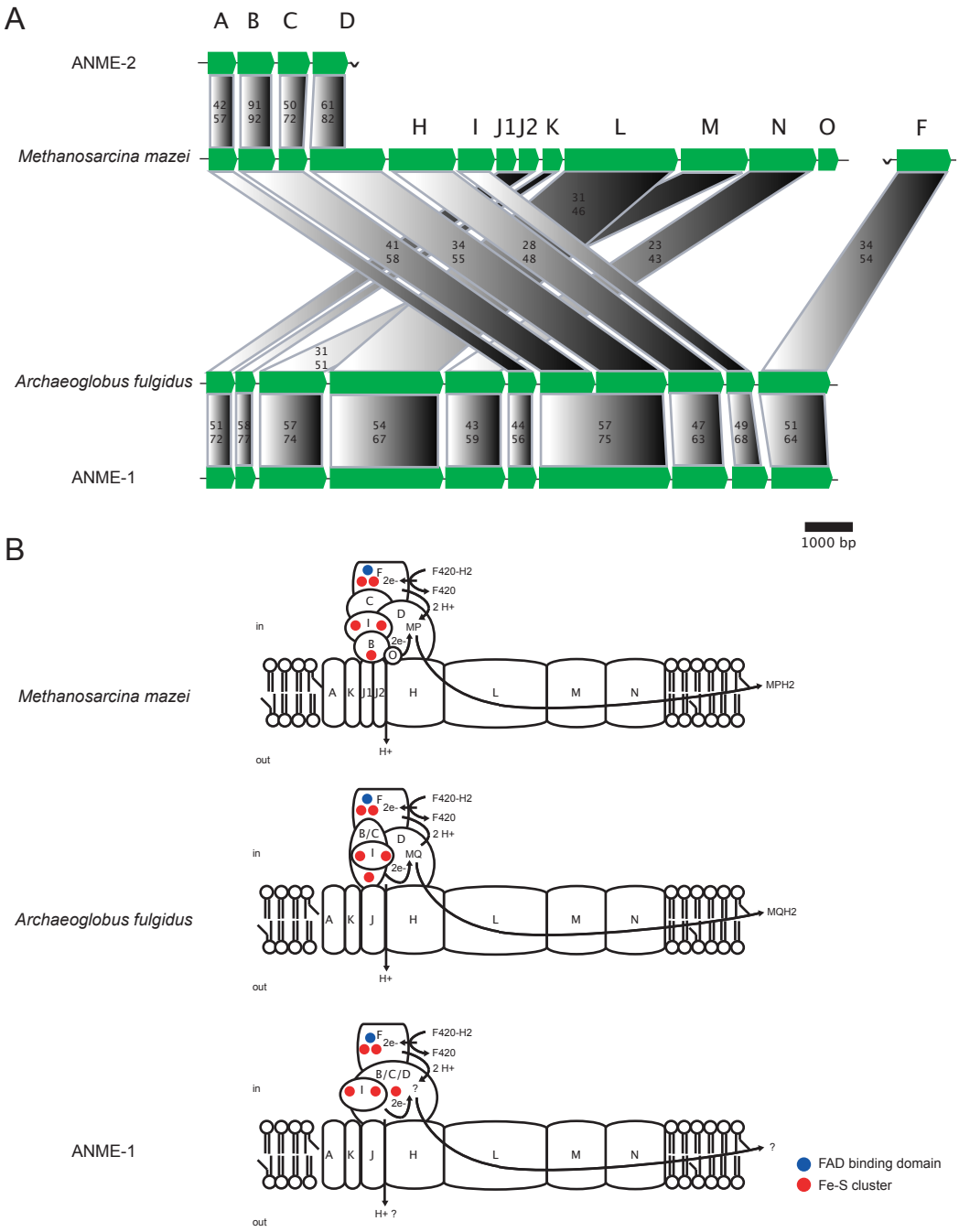

Fig. S3. Operonal structure and subunit relationships of F420-dependent quinone oxidoreductase (fqo) homologs from ANME-1 and ANME-2 archaea (A) Organization and subunit comparison of ANME-2 (top) and ANME-1 (bottom) fqo-related operons including nearest neighbors M. mazei and A. fulgidus. Percent identity (top) and similarity (bottom) between subunits shown in shaded areas. In cases of gene fusion (B/C/D, B/C, J) identity and similarity are represented by the average of combined subunit scores. (B) Tentative model for complex assembly and function in M. mazei, A. fulgidus and ANME-1 (reviewed in (6)). Although the electron acceptor in the ANME-1 case is unknown, the close relationship between A. fulgidus and ANME-1 complexes suggests a modified quinone. MP = methanophenazine. MQ = menaquinone.

Supplementary Table 1. Accession number index for SSU rRNA and *mcr* gene trees

#	Lineage	Organsism	Tree Code	Genbank Accesion No.						
				SSU	*mcrA*	*mcrB*	*mcrC*	*mrtC*	*mcrD*	*mcrG*
1	Methanosarcinales	*Methanococcoides burtonii*	Mbu	X65537	AAC43406	-	-	-	-	-
2	Methanosarcinales	*Methanosarcina mazei*	Mma	U20151	AAM30936	AAM30940	AAM30938	AAM30613	AAM30939	AAM30937
3	Methanosarcinales	*Methanosarcins barkeri*	Mba	M59144	ZP_00079263	ZP_00079259	ZP_00079261	ZP_00077727	ZP_00079260	ZP_00079262
4	Methanosarcinales	*Methanosaeta concillii*	Mco	X16932	AAK16832	-	-	-	-	-
5	Methanosarcinales	*Uncultured methanogen ODP8 ME2*	ODP8 ME2	-	AAD45632	-	-	-	-	-
6	Methanosarcinales	*Uncultured methanogen ODP8 ME6*	ODP8 ME6	-	AAD43406	-	-	-	-	-
7	ANME-2b	*Eel River uncultured archaeaon*	Eel-36a2B9	AF354140	-	-	-	-	-	-
8	ANME-2b	*Eel River uncultured archaeaon*	Eel-36a2A4	AF354128	-	-	-	-	-	-
9	ANME-2a	*Eel River uncultured archaeaon*	BA2H11	AF134393	-	-	-	-	-	-
10	ANME-2c	*Eel River uncultured archaeaon*	Eel-36a2A5	AF354133	-	-	-	-	-	-
11	ANME-2c	*Eel River uncultured archaeaon*	Eel-36a2A1	AF354129	-	-	-	-	-	-
12	ANME-2C	*Eel River uncultured archaeaon*	GZfos35D7	-	AAQ63481	AAQ63477	AAQ63479	-	AAQ63478	AAQ63480
13	ANME-2?	*Uncultured methanogen ODP8 ME1*	ODP8 ME1	-	AAD45631	-	-	-	-	-
14	Methanomicrobiales	*Methanoculleus thermophilcus*	Mth	M59129	AAK16834	-	-	-	-	-
15	Methanomicrobiales	*Methanospirrilium hungatei*	Mhu	M60880	AAK16835	-	-	-	-	-
16	ANME-1	*Guaymas uncultured archaeaon*	AF419626	AF419626	-	-	-	-	-	-
17	ANME-1	*Guaymas uncultured archaeaon*	AF419655	AF419655	-	-	-	-	-	-
18	ANME-1	*Black Sea uncultured archaeaon*	CAE46369	-	CAE46369	-	-	-	-	-
19	ANME-1	*Eel River uncultured archaeaon*	Eel-36a2G10	AF354137	-	-	-	-	-	-
20	ANME-1	*Eel River uncultured archaeaon*	EelRive2	submitted	-	-	-	-	-	-
21	ANME-1	*Eel River uncultured archaeaon*	BA1a2	AF134381	-	-	-	-	-	-
22	ANME-1	*Eel River uncultured archaeaon*	BA2f4	AF134392	-	-	-	-	-	-
23	ANME-1	*Eel River uncultured archaeaon*	GZfos17A3	-	AAQ63476	AAQ63474	AAQ63470	-	-	AAQ63475
24	Methanobacteriales	*Methanobacterium bryanti*	Mbr	M59124	AAK16836	-	-	-	-	-
25	Methanobacteriales	*Methanothermobacter thermautotrophicus*	Mthe12	Z37156	AAB85653	AAB85657	AAB85655	AAB85669	AAB85656	AAB85654
26	Methanococcales	*Methanocaldococcus jannaschii*	Mja	M59126	AAB98851	AAB98847	AAB98849	AAB98074	AAB98848	AAB98850
27	Methanococcales	*Methanococcus vannielii*	Mva	M36507	AAA72598	AAA72594	AAA72596	-	AAA72595	AAA72597

- Sequence unavailable or not included in present study

Supplementary Table 2. Fosmid Index and G+C-bin Summary

#	JGI	GZfos	bp	reads˅	GC	Depth†	bin*	Methanogenic Gene Id[a] 1	2	3	4
1	3436005	17G11	16872	68	0.440	4.03	I	*fmdA*			
2	3436025	23H9	39050	131	0.426	3.36	I	*fmdA*			
3	3436035	26D6	40124	102	0.439	2.54	I	*fmdC*	*hdrAA*	*frhB*	*frhD*
4	3436040	27B6	35761	76	0.435	2.14	I	*fmdC*	*cdhEDC*		
5	3436042	27E7	38891	12	0.426	0.31	I	*fmdAC*	*frhB*		
6	3436016	21B5	19184	152	0.449	7.95	I	*fmdDBAC*			
7	3634203	35A2	36677	98	0.437	2.69	I	*fmdE*			
8	3436051	32E4	35934	181	0.438	5.05	I	*ftr*	*fqoLNADHIF*		
9	3436069	36D8	37366	247	0.436	6.62	I	*ftr*	*fqoDHIF*		
10	3436671	17C7	37318	143	0.439	3.84	I	*ftr*	*fqoJKMLNADHIF*		
11	3435991	10C7	25292	87	0.454	3.46	I	*mch*			
12	3436039	27G5	40522	141	0.457	3.48	I	*mch*	SSU		
13	3436647	12E1	18559	83	0.474	4.52	I	*mch*	SSU		
14	3436647	12E1	16641	41	0.405	2.23	I				
15	3634190	19C8	30289	90	0.438	2.99	I	*mch*	*hdrBC*		
16	3435972	3D4	34178	11	0.438	0.33	I	*mtd*			
17	3436052	32E7	39737	99	0.433	2.50	I	*mtd*			
18	3436056	33E1	40093	113	0.425	2.83	I	*mtrEDCBAAGH*	*mrtC*	*frhB*	
19	3436064	34H9	38421	66	0.421	1.72	I	*mtrEDCBAAGH*	*mrtC*	*frhB*	
20	3634184	12E2	34628	116	0.427	3.36	I	*mtrEDCBAAGH*	*mrtC*	*frhB*	
21	2773121	34A6	36670	105	0.422	2.87	I	*mtrAAGH*	*Fe-S*		
22	3436000	14B8	36647	98	0.438	2.70	I	*mtrH*	*frhB*		
23	3436645	37D1	38721	51	0.419	1.34	I	*mtrH*	*frhB*		
24	3634188	18B6	10821	42	0.438	3.89	I	*mcrA*			
25	3634188	18B6	26805	53	0.421	2.01	I	*cdhAB*	*frhB*		
26	3435998	13E1	35492	140	0.424	3.95	I	*mcrBGA*			
27	3436026	24D9	29650	104	0.435	3.53	I	*mcrBGA*	*cdhAB*	*frhB*	
28	3435985	9E5	39717	105	0.419	2.66	I	*mcrCB*			
29	2773102	17A3	37604	87	0.443	2.33	I	*mcrCBGA*			
30	3435995	11H11	36155	149	0.435	4.14	I	*mcrCBGA*			
31	3436057	33H6	34700	150	0.431	4.35	I	*mcrCBGA*			
32	3436643	30H9	36779	140	0.431	3.81	I	*mcrCBGA*			
33	3634178	9C4	38084	69	0.433	1.82	I	*mcrCBGA*			
34	3634179	19C7	6963	15	0.475	2.15	I	*mcrCBGA*			
35	3634179	19C7	26540	76	0.434	2.89	I	*mcrG*			
36	3436038	26F9	22511	88	0.430	3.93	I	*hdrB*			
37	3436041	27E6	38634	141	0.423	3.67	I	*hdrB*			
38	3634189	19A5	37305	128	0.435	3.43	I	*hdrB*			
39	3634197	26D8	42166	155	0.433	3.69	I	*hdrB*			
40	3634206	9D1	33548	116	0.435	3.46	I	*hdrB*			
41	3436045	28G7	38396	236	0.438	6.16	I	*hdrCBA*	*Fe-S*		
42	3436049	29E12	29001	195	0.418	6.73	I	*hdrCBBA*			
43	3634193	23H7	30566	46	0.435	1.51	I	*Fe-S*			
44	3634198	28B8	36307	208	0.433	5.75	I	*Fe-S*			
45	3436033	26G2	44935	96	0.439	2.15	I	*cdhA*	*acd*		
46	3435986	9D8	40390	54	0.427	1.35	I	*cdhAB*	*frhB*		
47	3436065	34H10	29777	152	0.432	5.10	I	*cdhAB*	*frhB*		
48	2773118	35B7	38878	115	0.427	2.96	I	*cdhDE*	*frhB*		
49	3436009	18H11	36844	74	0.442	2.03	I	*cdhDE*			
50	3436654	32G12	16929	86	0.432	5.13	I	*acd*			
51	3436021	22D9	17825	30	0.432	1.69	I	*acd*			
52	2773119	25D1	20693	39	0.420	3.79	I				
53	2773119	25D1	10332	45	0.483	4.38	I	SSU			
54	3435991	10C7	11604	70	0.475	6.06	I	SSU			
55	2773114	34G5	11327	44	0.437	3.90	I				
56	2773114	34G5	23092	93	0.464	4.03	I	SSU	*cdhAC*		
57	-	1C11	42079	159	0.453	3.79	I	SSU	*cdhAC*		
58	3436666	37B2	45055	53	0.479	1.20	II	*fmdDB*	*cdhE*	*fpoDCBA*	
59	3436003	17F1	39756	8	0.500	0.23	II	*fmdE*	*cdhE*		
60	3436043	27A8	38133	12	0.471	0.34	II	*mcrBDC*	*fmdB*		
61	2773120	26B2	25119	35	0.506	1.43	II	*mcrDCGA*	*mch*		
62	2773122	35D7	25161	24	0.516	0.99	II	*mcrBDCGA*			
63	3435994	11A10	42686	40	0.485	0.94	II	*cdhAC*			
64	3436658	31B6	34272	13	0.490	0.39	II	*cdhA*			
65	3436665	1D1	28802	22	0.468	0.77	II				
66	3436665	1D1	16035	17	0.453	1.12	II	*acd*			
67	2773103	18C8	39495	24	0.505	0.63	II	SSU			
68	-	26E7	32690	24	0.520	0.76	II	SSU			

˅ Total number of matching shotgun reads (see methods)

† The density of WGS coverage of a fosmid clone is the number of full-length WGS read hits divided by the length of the fosmid sequence.

* Bin I corresponds to ANME-1 and bin II corresponds to ANME-2 archaeal groups

[a] Identification based on tblastN results constrained to expectation cut-off >E-10. Formylmethanofuran dehydrogenase (*fmd*), Formylmethanofuran:tetrahydromethanopterin formyltransferase (*ftr*), Methenyltetrahydromethanopterin cyclohydrolase (*mch*), Coenzyme F420-dependent N(5),N(10)-methenyltetrahydromethanopterin dehydrogenase (*mtd*), Methyltetrahydromethanopterin S-methyltransferase (*mtr*), Methyl coenzyme M reductase (*mcr, mrt*), CO dehydrogenase/acetyl-CoA synthase (*cdh*), Heterodisulfide reductase (*hdr*), Iron-sulfur protein (*FE-S*) Coenzyme F420-reducing hydrogenase (*frh*), Methylviologen F420-nonreducing hydrogenase (*mvh*), F420H2: phenazine oxidoreduxtase (*fqo, fpo*), ADP-forming Acetyl-CoA synthetase (*acd*)